Modeling of the N2+ ion in cold helium plasma: dynamics of N2+/He collisions and cross-sections

S Paláček, M Beseda, René Kalus, M Benhenni, Florent X. Gadéa, Thierry Leininger, Mohammed Yousfi

Modeling of the N_2^+ ion in cold helium plasma: dynamics of N_2^+/He collisions and cross-sections.

S Paláček[1,2], M Beseda[1], R Kalus[1,2], M Benhenni[3], F X Gadéa[4], T Leininger[4], and M Yousfi[3]

[1] IT4Innovations National Supercomputing Center, VŠB–Technical University of Ostrava, 17. listopadu 2172/15, 708 00 Ostrava–Poruba, Czech Republic

[2] Department of Applied Mathematics, Faculty of Electrical Engineering and Computer Science, VŠB–Technical University of Ostrava, 17. listopadu 2172/15, 708 00 Ostrava–Poruba, Czech Republic

[3] Laboratoire Plasma et Conversion d'Energie, LAPLACE & UMR5213 du CNRS, Université de Toulouse III Paul Sabatier, 118 route de Narbonne, 31062 Toulouse Cedex, France

[4] Laboratoire de Chimie et de Physique Quantiques, IRSAMC & UMR5626 du CNRS, Université Toulouse III – Paul Sabatier, 31062 Toulouse Cedex 09, France

E-mail: stanislav.palacek@vsb.cz, martin.beseda@vsb.cz, rene.kalus@vsb.cz, malika.benhenni@laplace.univ-tlse.fr, gadea@irsamc.ups-tlse.fr, thierry.leininger@irsamc.ups-tlse.fr

Abstract. A detailed dynamical study is presented for N_2^+/He collisions running in the electronic ground state of the collision complex. Hybrid, quantum-classical dynamical calculations have been performed considering a broad range of collision energies (E_{coll} = 0.01–100 eV) and various initial rotational-vibrational excitations of the N_2^+ ion. Both non-reactive and reactive (N_2^+ collision-induced dissociation) cross-sections have been calculated with the momentum-transfer approximation applied to the former ones. A thorough comparison with pseudo-experimental data obtained from mobility measurements reported in the literature via an inverse-method approach has been performed and the effect of the rotational alignment of the N_2^+ ion on calculated cross-sections has been assessed and analyzed.

1. Introduction

The interest in cold rare-gas plasmas is primarily motivated by their promising applications. Various areas have been mentioned in the literature, like biomedicine [1, 2, 3], agriculture and food production [4, 5], VUV light emission [6, 7], and others. Noteworthy, helium plays an important role in such applications. To make the applications as efficient as possible, a detailed understanding of plasmas properties is needed, both at the qualitative and quantitative level. For this, numerical modeling and simulations represent an indispensable tool since they are able to provide realistic data, mainly because of the rapid development of simulation methods and hardware resources seen in the last decade, which are quantitatively comparable with experiments but can be produced at much lower costs and with deeper insight. In this way, a goal of reaching a quantitative description of macroscopic properties of cold plasmas based exclusively on first-principles treatments becomes both very attractive and achievable.

The cold rare-gas plasmas are usually generated via a dielectric-barrier discharge ignited in a carrier rare gas by high voltage [8]. First, atomic as well as molecular (mainly diatomic) ions of the carrier rare gas are formed inside the plasma generator, carried downstream by the flowing carrier gas, and, finally, come into contact with the environment (air) upon the plasma jet leaves the generator. **Then, secondary ions are formed from the main constituents of air, nitrogen in particular. In the present paper, we specifically focus on the interaction of the N_2^+ ion with helium carrier gas.** In this way, our former calculations on collisions of atomic and molecular ions of helium with helium carrier gas [9, 10], occurring inside helium plasma generators, are extended to interactions of the plasma with environment upon the plasma leaves the generator. As a first step, adiabatic conditions and collisions running on the ground-state potential energy surface of the N_2^+/He complex are assumed. The role of electronically excited states of the complex and non-adiabatic transitions between them will be the subject of a future study.

At the microscopic level, two main reaction paths are expected to take place if a *molecular dynamics simulation* (MDS) is expected to run adiabatically on the ground-

state potential energy surface of the N_2^+/He collision complex, the more abundant *non-reactive scattering* (NRS),

$$N_2^+ + He \rightarrow N_2^+ + He, \tag{1}$$

and, due to the strong binding in the N_2^+ ion, much less frequent *collision-induced dissociation* (CID) of the ion,

$$N_2^+ + He \rightarrow N^+ + N + He. \tag{2}$$

A couple of other processes may also in principle appear but will not be considered here because of their marginal importance (as approved by our calculations). For example, a reaction of $N_2^+ + He \rightarrow [NHe]^+ + N$ may occur at high collision energies. However, it has not been detected in our simulations at all. Another example of similarly unimportant processes, which are not taken into account here, is $N_2^+ + He \rightarrow NHe + N^+$. This process has neither been observed in our calculations, mainly because of the extremely weak binding in the NHe complex. In addition to the two "exotic" collision processes mentioned above, the charge transfer channel, $N_2^+ + He \rightarrow N_2 + He^+$, may become important as the collision energy increases. However, it will also be ignored here because a) very high collision energies are needed for it to open ($E_{\rm coll} \gtrsim 10\,{\rm eV}$) due to a large difference of the ionization potentials of He and N_2, and b) highly excited electronic states of the N_2^+/He complex will have to be included, which goes beyond the scope of the present study.

It should be also noted that the understanding of the processes of activation and/or disintegration of colliding ions is of principal importance in mass-spectrometry experiments [11]. The results of the present study may thus be useful, though indirectly, in that field of research as well. It should be noted, however, that much higher collision energies (in the keV range) are considered in the mass-spectrometry experiments [12, 13] than those taken into account in the present work. Under such extreme conditions, electronically excited states of the N_2^+ and N^+ ions are produced. Since, on the other hand, the present work is exclusively focused on the ground-state dynamics of the N_2^+/He collision complex, its relevance for the field of mass spectrometry may be limited and will not be discussed below.

To numerically model the processes of Eqs. (1) and (2), a direct dynamics method [14], with energies and forces calculated on the fly using *ab initio* approaches, has been primarily used. In addition, analytic representations of *ab initio* potential energy surfaces have also been considered to get computationally cheap interaction models working at the accuracy basically comparable to the accuracy of high-level *ab initio* methods. For the latter, artificial intelligence approaches [15] based on the use of artificial neural networks [16] have been utilized.

The rest of the present paper is organized as follows. Immediately following this introductory part, computational methods are summarized in Sec. 2, including the treatment of collisional dynamics and models of interactions in N_2^+/He (Subsecs. 2.1

and 2.2, respectively), calculated cross-sections (Subsec. 2.3), and auxiliary inverse-method calculations for extracting pseudo-experimental cross-section data from mobility measurements of N_2^+ in helium (Subsec. 2.4), the latter being used to assess the accuracy of our numerical predictions. Finally, a summary of the main results and observations, and conclusive remarks are provided in Sec. 4.

2. Methods and computations

2.1. Dynamics

The MDSs have been performed on the ground-state potential energy surface of the N_2^+/He ion using a hybrid approach. It means that atomic nuclei have been treated classically while a full quantum treatment has been adopted for electrons. For the classical treatment of nuclei, Hamilton's equations of motion have been used,

$$\dot{\overrightarrow{r}}_k = \frac{\overrightarrow{p}_k}{m_k}, \;\; \dot{\overrightarrow{p}}_k = \overrightarrow{F}_k, \tag{3}$$

where $\overrightarrow{r}_k$, $\overrightarrow{p}_k$ and m_k are the position vector, linear momentum and mass of the k-th atom, respectively, $\overrightarrow{F}_k = -\nabla_k E$ is the force acting on the k-th atom, with E standing for the ground state potential energy surface (PES) calculated at the Born-Oppenheimer level.

The quasi-classical trajectory (QCT) approach [17] has been used to obtain bunches of trajectories to be further utilized in calculations of collision cross-sections. For each trajectory, a multi-step 4^{th} order method has been used to numerically integrate the classical equations of motion, Eq. (3). A predictor–corrector method of a prediction–evaluation–correction–evaluation (PECE) scheme [18] has been used with the Crane–Klopfenstein [19] and Adams–Moulton [20] methods used as the predictor and the corrector, respectively. To initialize the calculation, the classical 4^{th} order Runge-Kutta method [21] has been employed.

The initial conditions of Eq. (3) consist of a couple of parameters that are fixed for a particular bunch of trajectories and some other parameters which are allowed to vary across different trajectories included in the bunch, the latter being sampled from distributions corresponding to typical experimental conditions. The fixed parameters include the rotational-vibrational state of the N_2^+ ion given by its rotational, j, and vibrational, v, quantum numbers, and the N_2^+/He center-of-mass collision energy, E_{coll}, while the sampled quantities comprise the isotropic orientation of the N_2^+ ion in space, the phase of its vibrational motion, the orientation of the N_2^+ angular momentum in space, and the impact-parameter of the N_2^+/He collision.

The generation of initial conditions proceeds for particular values of j, v, and E_{coll} as follows. First, a grid of collision impact-parameters, b, ranging between $b = 0$ and $b = b_{\max}$ with $b_{\max}$ chosen iteratively in course of a calculation so that $b \geq b_{\max}$ contribute negligibly to any of the calculated cross-sections, is considered with a step

of $\Delta b = 0.4\,\text{bohr}$. For each value of the impact parameter, an ensemble of 128 initial conditions has been generated in a couple of subsequent steps. Firstly, the N_2^+ internuclear distance has been randomly assigned utilizing the probability distribution obtained from the square of the nuclear wave function of the selected rotational-vibrational state of the N_2^+ ion. The center of mass of the ion has been put to the origin of coordinates. Secondly, linear momenta of nitrogen atoms are adjusted so that the angular momentum of N_2^+ corresponds to the rotational quantum number of the selected state of the ion and its internal energy is equal to the eigenenergy of the selected rotational-vibrational state. Thirdly, the N_2^+ ion is randomly rotated in space, including the linear momenta added to the nitrogen nuclei. Fourthly, the position of the incoming He atom is adjusted in the x-z plane so that its x-coordinate corresponds to a particular value of the impact-parameter, $x_{\text{He}} = b$, and the z-coordinate is equal to a preset value $z = z_{\max}$ ($z_{\max} = 10\,\text{bohr}$ in the present calculations). The linear momentum of the He atom is assigned a value corresponding to the particular value of the N_2^+/He collision energy, E_{coll}, transformed from the center-of-mass of the collision complex to the current frame (linked to the center of mass of the N_2^+ ion). Finally, the coordinates and momenta of all the three atoms are transformed to the center-of-mass system of the N_2^+/He collision complex.

To create a particular rotational-vibrational state in the N_2^+ ion prior to its collision with He, corresponding rotational-vibrational wave function and energy level are needed. They have been calculated using the LEVEL16 package [22] and an N_2^+ potential calculated at the same level of theory as used in dynamical calculations (see Subsec. 2.2). Cubic splines have been used to interpolate between discrete *ab initio* points.

Each particular trajectory has been evolved numerically until a distance-based termination criterion is met. Specifically, a calculation is terminated if at least two of the three distances between the nuclei of the N_2^+/He complex become larger than the maximum of the three distances recorded at the beginning of the calculation. If all three distances exceed this limit, the CID channel is considered to take place. Otherwise, the stability of the resulting diatom, which has exclusively been the N_2^+ ion in our calculations, is tested using its internal energy. If the internal energy is below the dissociation limit, the NRS channel is considered on the output, otherwise the CID channel is assumed to take place. In this way, final coordinates of the colliding particles and their momenta have been obtained to be used in subsequent cross-sections evaluations (see Sec. 2.3).

It should be noted that for collision energies $E_{\text{coll}} \lesssim 0.1\,\text{eV}$, long-lived, "orbiting" trajectories have been encountered for specific values of the impact parameter, which has led to considerably increased computational times. To meet wall-time limits imposed by the computational resources we used in our calculations, another termination criterion has been adopted for such cases consisting c) in checking the maximum time of computation and repeatedly chaining calculations until the distance-based conditions (a and b) are obeyed.

All the MDSs reported in this study have been performed using homemade

codes [23] in which both the dynamical part of the calculations and necessary interfaces to third-party electronic structure codes are implemented. Communication with the electronic structure codes has been performed by sharing messages and data exchanged via files saved to a fast hard drive and/or RAM disk. Most of the implementation has been written in the Fortran 90 language with an envelope of bash scripts used to implement the interfaces.

2.2. Interactions

A key input to any MDS is the calculation of forces (energy gradients) acting between interacting particles. In the present work, most of the MDSs have been performed in the *direct dynamics* regime [14] with the forces and energies calculated via *ab initio* methods employed on the fly. For this, standard methods of quantum chemistry have been used as implemented in the MOLPRO software package [24], versions *mpp-2020.1.2* and *mpp-2021.1*.

The main working tool of the present study has been the *multi-configuration self-consistent field* (MCSCF) method [25, 26]. In a preceding study [27], we analyzed the performance of the MCSCF method by comparing it with the more accurate *multi-reference configuration interaction* (MRCI) approach, both for the N_2^+ ion and the N_2^+/He collision complex, and showed that it provided a sufficient level of accuracy while leading to acceptable computational costs. As a consequence, the MCSCF method is selected here to serve as a suitable trade-off between accuracy and computational feasibility if applied on the fly.

All the electronic structure calculations have been performed for the electronic ground state of the N_2^+/He complex in the state-specific regime. An aug-cc-pVQZ (avqz) basis set [28, 29] has been utilized to properly describe induction interactions between the weakly polarizable He atom and the N_2^+ ion. The g-orbitals, inherently included in the quadruple-zeta basis sets, have been omitted in order to make the use of analytical gradients possible in the used versions of the MOLPRO package and to avoid time-consuming numerical calculations of forces. Hereafter, the reduced basis set will be denoted as avqz(spdf).

The orbital space (OS) adopted for the MCSCF calculations on the base of thorough testings [27] consists of eleven A' and two A" functions, i.e., the minimal active space has been used with two more A' orbitals added to better describe the anisotropic distribution of the positive charge in the N_2^+ ion. Such an OS improves the numerical accuracy while the computational demands still remain feasible. Moreover, as was shown in Ref. [27], the use of the MCSCF method combined with the moderate basis set and the OS considered in this work leads to an accuracy comparable with the accuracy of benchmark MRCI calculations, in contrast to big basis sets and extensive OSs when worse agreement with the benchmark calculations is achieved[1].

1 To make these extensive tests employing larger basis sets (up to aug-cc-pV6Z) and orbital spaces including all the 3p orbitals of nitrogen (in addition to the 3s ones considered in this work) practicable,

Because of the high computational demands of the *ab initio* methods, an alternative approach based on artificial neural networks (ANNs) has been employed to save computer time in **some dynamical calculations performed in the present work**. Specifically, the use of an ANN representation of the PES of a system is expected to provide a much less computationally demanding interaction model which may be, on the other hand, of comparable quality as the underlying *ab initio* calculation used to generate data against which the ANN has been trained. Basically, any accuracy of quantum chemical calculations may be reproduced in this way at considerably reduced computational costs.

In our work, fully connected, feed-forward ANNs have been used as implemented in a homemade code developed recently in our group (*neuron4dyn*). ANNs with four layers comprising an input layer with three neurons representing coordinates of the N_2^+/He collision complex (see below), two hidden layers containing twenty and five neurons, respectively, and an output layer providing the interaction energy of the complex have been used. Standard logistic activation functions have been assigned to the neurons in hidden layers while linear activation is used in both the input neurons and the output neuron. The ANNs have been trained **against data collected as a "side product" of** the MDSs performed in the on-the-fly regime.

It should be emphasized here that it is not the aim of the present work to develop a general-purpose ANN representation of the N_2^+/He **ground-state PES. Instead, computationally cheap models of the PES have been developed which reproduce the underlying *ab initio* data as close as possible. For this reason, separate ANNs have been trained for each collision energy**[2] using a training method based on a Kalman filter approach [30]. In this way, a set of $E_{\rm coll}$ **specific ANNs have been obtained which almost identically reproduce all the parts of the** N_2^+/He **ground-state PES relevant for the specific value of** $E_{\rm coll}$. Typically, hundreds of thousands to millions of points collected during dynamical simulations [3] have been used as training sets, which ensures a very high fidelity of the resulting ANNs.

The quality of the developed ANNs is justified by insignificant deviations between the training energies and the estimates returned by the ANNs. Typically, the deviations are well below 1 meV for **the ANNs developed for** $E_{\rm coll} \leq 1\,\mathbf{eV}$**, up to 5 meV for** $\mathbf{1\,eV} < E_{\rm coll} \leq 15\,\mathbf{eV}$**, and only exceed this value for the highest collision energies considered (**$E_{\rm coll} \geq 20\,\mathbf{eV}$**). The mean absolute errors (MAEs) are** $\lesssim 0.2\,\mathbf{meV}$, $\lesssim 1.2\,\mathbf{meV}$**, and about 4−5 meV, respectively. Note that much less favorable results would have been obtained if a general ANN had been**

they were only performed for the N_2^+ ion, the most difficult part of the N_2^+/He complex.

2 In the present work, only the j=0,v=0 initial state of the N_2^+ ion has been considered for the developed ANNs.

3 The number of training points depends on the dynamical data collected for particular collision energies, the number decreases with increasing $E_{\rm coll}$. For example, 2×10^6 to 4×10^6 training points have been available for the smallest two collision energies while 10^5 to 7×10^5 points have been used for $E_{\rm coll} \geq 0.15$ eV.

trained using the same ANN architecture and/or considerably bigger ANNs should have been used. For example, if the data sets obtained for the highest collision energies ($E_{\rm coll} \geq 20\,{\rm eV}$), which cover the largest part of the N_2^+/He PES, are used to train an ANN of the same architecture as employed in this work, typical MAEs amount to about 2−7 meV for the points generated for $E_{\rm coll} \leq 1\,{\rm eV}$ and to about 5−14 meV for $1\,{\rm eV} < E_{\rm coll} \leq 15\,{\rm eV}$. This means that at least by an order of magnitude worse accuracy is achieved in this case for the most relevant range of collision energies[4].

Permutational invariant polynomials of reciprocal values of distances between atomic nuclei in the N_2^+/He complex, $f_1(r_1, r_2, r_3) = r_1^{-1}$, $f_2(r_1, r_2, r_3) = r_2^{-1} + r_3^{-1}$, $f_3(r_1, r_2, r_3) = r_2^{-2} + r_3^{-2}$, with r_1 being the internuclear distance between nitrogen atoms and r_2 and r_3 representing the distances between the helium atom and nitrogen atoms, have been used as the input to the ANNs. As a consequence, not only translational and rotational invariance of the resulting PES is assured, but also permutational invariance with respect to the exchange of the two nitrogen atoms is included.

2.3. Cross-sections

As mentioned in Sec. 1, the collisions of interest in this work are the N_2^+/He *non-reactive scattering* (NRS), Eq. (1), and the *collision-induced dissociation* (CID) of the N_2^+ ion, Eq. (2). The basic quantity used to quantitatively describe these collision processes is the differential cross-section, $\mathrm{d}\sigma/\mathrm{d}\Omega$. However, the differential cross-section of the former process cannot be directly used since, within the classical approach, the differential cross-section of the NRS process has a non-integrable singularity at the zero deflection angle and, thus, the corresponding integral cross-section diverges.[5]

To deal with this problem, approximate cross-sections calculated at the momentum-transfer approximation level [32], momentum-transfer cross-sections (MTCSs), are used. Following our previous studies (see, e.g., Ref. [33]), two types of MTCSs have been considered,

$$\sigma_{\rm NRS}^{\rm (MT1)} = \int_{4\pi} \left[\frac{\mathrm{d}\sigma}{\mathrm{d}\Omega}\right]_{\rm NRS} (1 - \cos\theta)\,\mathrm{d}\Omega, \tag{4}$$

$$\sigma_{\rm NRS}^{\rm (MT2)} = \int_{4\pi} \left[\frac{\mathrm{d}\sigma}{\mathrm{d}\Omega}\right]_{\rm NRS} \left(1 - \frac{p'}{p}\cos\theta\right)\mathrm{d}\Omega, \tag{5}$$

where θ is the scattering angle, p and p' are the magnitudes of the linear momentum of the He atom before and after the collision, respectively, and $[\mathrm{d}\sigma/\mathrm{d}\Omega]_{\rm NRS}$ denotes the differential cross-section of the NRS channel. Hereafter, we will denote the two types of cross-sections as MTCS1 (or, alternatively, "type 1 MTCS") in the case of Eq. (4) and MTCS2 (or "type 2 MTCS") for Eq. (5). It is noteworthy that the presence of

4 As follows from our preliminary calculations and will be discussed in a following work [31], N_2^+/He collision energies are well below 15 eV if an external electric field up to $E/N \approx 200\,{\rm Td}$ is applied.

5 The NRS process comprises the elastic scattering channel which has, at the classical limit, an infinite integral cross-section. As a consequence, the same holds for the NRS channel.

the cosine terms in integrals on the right-hand side of Eqs. (4) and (5) suppresses the divergence of the differential cross-section at $\theta \to 0$ and the resulting MTCSs are finite. As discussed before [9], the use of the momentum-transfer approximation introduces only a negligible error. Note also that MTCS1 was originally introduced for elastic scattering while MTCS2 represents a generalized version presumably better describing non-elastic processes accompanied by a transfer of energy between translational and internal degrees of freedom. Both approaches were successfully tested in a series of previous calculations on rare-gas ionic diatom/atom collisions reported from our group (see, e.g., Refs. [34] and [35] and references given therein).

For the CID process, a process with a non-zero energetic threshold, such problems do not occur, and a standard integral cross-section,

$$\sigma_{\mathrm{CID}}^{(\mathrm{int})} = \int_{4\pi} \left[\frac{\mathrm{d}\sigma}{\mathrm{d}\Omega}\right]_{\mathrm{CID}} \mathrm{d}\Omega, \tag{6}$$

may be used even at the classical level.

In order to check the convergence of cross-sections with respect to the impact-parameter and to properly choose the maximum value of the impact-parameter, $b_{\max}$, for a particular [E_{coll},j,v] calculation, an auxiliary quantity representing (dimension-less) contributions to the considered cross-sections from trajectories started at a particular value of the impact-parameter, $\Delta\sigma_{\mathrm{X}}^{(\mathrm{Y})}(b)$ (X = NRS or CID, and Y = MT1, MT2 or int), has been introduced by

$$\sigma_{\mathrm{X}}^{(\mathrm{Y})} = \int_0^{+\infty} 2\pi b \Delta\sigma_{\mathrm{X}}^{(\mathrm{Y})}(b)\mathrm{d}b. \tag{7}$$

For each calculation, we observed the evolution of $\Delta\sigma$ with b for both NRS and CID and set $b_{\max}$ so that $2\pi b\Delta\sigma(b) \approx 0$ for both channels at $b \geq b_{\max}$.

2.4. Inverse-method calculations

To our best knowledge, no experimental data have been reported in the literature for N_2^+/He for either NRS or CID cross-sections. As a consequence, it is not possible to directly compare the data calculated within the present work with experiment. For MTCS1, however, pseudo-experimental estimates of the cross-section can be extracted from measured mobility of the N_2^+ ion in helium gas [36] via a so-called *inverse method* [8]. Following a good practice of our preceding studies [8, 34, 35], we use this approach to calculate type 1 MTCSs to serve as "experimental" benchmarks for testing our theoretical approaches.

The *inverse method* (IM) [36, 37] is an approximate computational approach using a simple spherical core potential to describe the interactions between the colliding particles (which are considered to be structure-less and point-wise),

$$V_{core} = \frac{n\epsilon_w}{3n-12}\left[\frac{12}{n}\left(\frac{r_m-a}{r-a}\right)^n - 3\left(\frac{r_m-a}{r-a}\right)^4\right], \tag{8}$$

with n, ϵ_w, r_s, and r_m being adjustable parameters to be optimized against available (experimental) data, usually the ion mobility in buffer gas measured over a sufficiently broad range of the reduced electric field. The method starts with setting a plausible *ansatz* for the core-potential parameters and then typically proceeds through three iterative steps: a) MTCS1 calculations[6] based on Jeffreys-Wentzel-Kramers-Brillouin (JWKB) method [38], b) mobility calculations utilizing the cross-sections obtained in the preceding step and employing, e.g., Monte Carlo simulations [39], and c) the readjustment of the core-potential parameters based on the comparison of calculated and measured (mobility) data. These three steps are repeated until a good correspondence between experimental and calculated data is achieved.

3. Results and discussions

3.1. Inverse-method calculations

Prior to presenting the data calculated within this work, let us briefly discuss how their accuracy has been tested and justified. As mentioned above, to our best knowledge, no direct measurements have been reported in the literature for the cross-sections of the NRS of N_2^+/He nor for the CID cross-sections. As a consequence, only indirect comparisons with experiments can be made using pseudo-experimental values of MTCS1 obtained from N_2^+/He mobility measurements via the inverse method approach described in Subsec. 2.4.

A survey of the most extensive experimental data on the N_2^+/He mobility [40, 41, 42] is provided in the inset of Fig. 1, related type 1 MTCSs derived from the IM are shown in the main panel of the figure, **and for comparison, the** N_2^+/He **mobility values calculated from the IM cross-sections are also shown in the inset**. Looking at the inset of the figure, one can clearly see that different experimental mobility points are rather close to one other, so, their reliability is mutually verified. Just the most recent measurement by Anthony et al. [42] are slightly above the older ones by McFarland et al. [40] (in this work we use the values reported in a compilation by Ellis et al. [43]) and Kaneko et al. [41]. **The IM representations of the** N_2^+/He **mobility also perfectly agree with one another as well as with the experimental points. Mainly the latter correspondence clearly shows a good performance of the IM in the specific case of the** N_2^+/He **scattering, at least** over the range of the reduced electric field considered in the experiments. **The resulting IM** type 1 MTCSs (shown in the main panel) may thus be considered a realistic substitute of missing experimental data[7]. **As mentioned above, a similarly favorable performance of the IM**

6 Since a simple interaction potential is used, which does not take into account either the CID channel or the non-elastic scattering, only type 1 MTCS can be calculated in this way. The simplifications used in the IM method may, in addition, lead to a serious failure of the method if very strong electric fields are involved in which both neglected processes may become important.

7 Since the IM approach cannot be used to calculate the CID cross-sections, which are neither available in the literature, we will exclusively rely on tests based on the comparison of MTCS data in this work.

approach was also observed in our preceding studies [8, 34, 35], which further supports the use of the IM cross-sections as a reliable pseudo-experimental benchmark.

3.2. Momentum-transfer cross-sections

A summary of the MTCSs we have obtained is provided in Fig. 2. Specifically, MTCS1 is considered in this figure. Note that various initial vibrational and/or rotational excitations of the N_2^+ ion have been taken into account. Firstly, the rotational-vibrational ground state of N_2^+ (j=0,v=0) has been included as a representative of a thermal population[8] of the ion at $T = 300$ K. Secondly, j=0,v=1 (about +0.27 eV above the ground state at the MCSCF/avqz(spdf) level) is used to represent low-lying vibrational states of the N_2^+ ion and to see the effect of its vibrational excitation. Thirdly, j=36,v=0 represents a rotationally excited state of the N_2^+ ion with the excitation energy (about +0.31 eV) close to the j=0,v=1 case. It is included to see the difference between calculated cross-sections when the excitation energy is pumped into the vibrational degrees of freedom of the N_2^+ ion and the case when the rotation of the ion is enhanced by a comparable amount of energy. Finally, a rather high vibrational excitation of j=0,v=10 (about +2.5 eV above the ground state) has been included to see the effect of the highest N_2^+ vibrational excitations for which the adiabatic approximation adopted in this work is valid[9].

The most important observations one can draw from Fig. 2 are as follows. Firstly, a very good agreement between the theoretical data and IM calculations is seen for $E_{\rm coll} \approx 0.05 - 1.0$ eV. This is particularly well apparent if the theoretical data are compared with the IM values obtained from the most recent experiment [42]. Secondly, for low collision energies (here represented by $E_{\rm coll} = 0.01$ eV), a well apparent deviation is seen between theory and IM. The theory underestimates the IM cross-section by about 4–5 times, probably because the MCSCF method does not describe the long-range polarization forces acting between the N_2^+ ion and the He atom at long distances with a sufficient accuracy. **These long distances get particularly important at very low collision energies. It is illustrated in Fig. 3 where contributions of different impact parameters (see Eq. (7)) to the type 1 MTCSs are depicted for the specific case of j=0,v=0 and selected collision energies. Clearly, impact parameter values up to $b_{\rm max} \approx 11$ bohr contribute for the lowest energy considered ($E_{\rm coll} = 0.01$ eV) while significantly smaller values**

8 At room temperature, the vibrational state of the N_2^+ ion is dominantly $v = 0$ (as estimated from equilibrium statistics) and only low-lying rotational states are occupied with the mean rotational quantum number being $\langle j \rangle \approx 10$.

9 Slightly above the j=0,v=10 excitation energy, a crossing occurs between the ground state ($X^2\Sigma_g^+$) and the lowest excited state ($A^2\Pi_u$) of the N_2^+ ion and the adiabatic approximation may thus fail for these high excitation energies.

of $b \lesssim 5.5 - 7.5$ bohr are important for higher collision energies ($E_{\rm coll} = 0.05$ eV and $E_{\rm coll} = 0.15$ eV). Highly probably, *ab initio* methods with a more accurate inclusion of dynamical electronic correlations will be needed to remove this discrepancy. For example, the MRCI method may be an appropriate choice. Thirdly, a similar, though less dramatic (if the logarithmic scale on the cross-section axis is taken into account) disagreement is also seen between calculated and IM cross-sections at the highest collision energies included in Fig. 2. However, it is not clear whether the approximate IM provides reliable results in this high-energy region. Fourthly, the effect of the initial rotational-vibrational excitation in the N_2^+ ion on the resulting MTCS data is only marginal. Interestingly, it holds even for rather highly vibrationally excited ions (j=0,v=10), the linear dimension of which and, as a consequence, corresponding geometric cross-sections are non-negligibly increased.

Another important question, namely what will be the difference between data obtained using type 1 (Eq. (4)) and type 2 (Eq. (5)) MTCSs, is examined in Fig. 4. The data depicted in this figure clearly show that both methods of MTCS calculations yield basically the same results, the deviations being (mostly considerably) below 0.6 Å^2, even for the largest N_2^+ rotational-vibrational excitation and highest collision energies for which inelastic processes might be expected to play a role. However, it seems that the opposite is true and that the transfer of energy between translational degrees of freedom of the N_2^+/He complex and the rotational-vibrational degrees of freedom of the N_2^+ ion is not much important. As a consequence, only the type 1 MTCS will be used in the following analysis and discussion.

As mentioned before, nor experimental neither theoretical data exist for the N_2^+/He cross-sections in the literature we could directly compare with. An indirect comparison and validation of the present data can be however performed using integral cross-sections of the vibrational excitation/de-excitation of the N_2^+ ion in collisions with low-energy electrons (Ecoll $\lesssim 2.3$ eV) calculated recently via a *Multichannel Quantum Defect Theory* method [44]. Despite the facts that a) the collisions studied here, N_2^+/He, and those of Ref. [44], N_2^+/e^-, are rather different from each other, b) different kinds of cross-sections have been considered (integral vs. momentum-transfer), and c) the levels of calculations of both studies differ considerably, it is encouraging that the values reported in Ref. [44] compare rather well with ours. For example, it can be learnt from Fig. 3 of Ref. [44] that the cross-sections of $N_2^+(v = 0) + e^- \rightarrow N_2^+(v = 1) + e^-$, a dominating channel of the $N_2^+(v = 0)/e^-$ collision, range between 1 Å^2 and 30 Å^2 around $E_{\rm coll} \approx 0.5$ eV, and between 1 Å^2 and 18 Å^2 for $E_{\rm coll} \approx 1.0$ eV. The estimates we obtained for the same collision energies for N_2^+/He are about 14 Å^2 and 12 Å^2, respectively, with both values matching well the experimental N_2^+/e^- spans. For higher collision energies, $E_{\rm coll} \approx 1.5$ eV and $E_{\rm coll} \approx 2.0$ eV, the values of Ref. [44] ($\lesssim 4$ Å^2 and $\lesssim 2$ Å^2, respectively) are, on the other hand, well below our estimates (about 10 Å^2 and 9 Å^2, respectively). In the higher-energy region,

the methodological differences between the calculations of Ref. [44] and the present ones seem thus to have much better pronounced effect. But, even though and rather encouragingly, both data sets remain rather close to each other.

3.3. Dissociation cross-sections

It is not much to be said about the cross-section of the N_2^+/He CID except that it is very small over the whole range of collision energies and for all the N_2^+ rotational-vibrational excitations considered, as is clearly seen from Fig. 5. Interestingly, even for the highest N_2^+ vibrational excitation (j=0,v=10), the CID cross-section is always below about 0.8 Å^2, like for the two lower excitations considered here as well as for the rotationally-vibrationally ground state of the N_2^+ ion. Naturally, the energetic threshold of the N_2^+ CID decreases as the excitation of the N_2^+ ion grows up, but the values of the CID cross-section increase only marginally. In conclusion, the CID channel plays a minor role in N_2^+/He collisions, highly probably due to a rather big difference between the masses of helium and nitrogen atoms.

3.4. The effect of N_2^+ alignment

Since the interaction of the N_2^+ ion with He is strongly anisotropic, the effect of the collision-induced alignment of the angular momentum [45] of N_2^+ ions is expected to be important in N_2^+/He collisions, as previously suggested by experiments [46, 47] as well as simulations [48, 49, 50]. In this subsection, we briefly analyze the effect of the N_2^+ alignment on calculated cross-sections. To save computer time, ANNs trained against the data obtained from preceding on-the-fly calculations have been employed rather than running additional computationally demanding on-the-fly calculations.

The effect of the N_2^+ alignment on the cross-sections reported in this work is analyzed for the specific case of the rotationally-vibrationally ground-state N_2^+ ion (j=0,v=0). For this, fully-connected, feed-forward ANNs **of a 3−20−5−1 architecture (see Subsec. 2.2) have been specifically built** for each collision energy considered. In this way, highly accurate representations of specific domains of the N_2^+/He potential energy surface which are relevant for at particular collision energies have been obtained. As an illustration of achieved accuracy, in Fig. 6 we provide a comparison between cross-sections obtained for N_2^+(j=0,v=0) from the on-the-fly calculations and from additional calculations employing the optimized ANNs. Clearly, the agreement between the two calculations is excellent and the accuracy of the ANNs is thus fully warranted **for the purposes of the present calculation**.

The effect of the N_2^+ angular momentum (J) alignment in N_2^+/He collisions is illustrated, for the specific case of j=0,v=0, in Fig. 7 where cross-sections calculated for parallelly (PAR) and perpendicularly (PER) oriented J are compared with data obtained for non-aligned J (NA). An explanatory note should be added here specifying more clearly how different alignments of the N_2^+ ion angular momentum have been

modeled in the specific case of the rotational ground state of the N_2^+ ion (for which the ion angular momentum is zero). In this case, specific alignments of the N_2^+ itself are considered. Without loss of generality, one may suppose that the center of mass of the ion is put, at the beginning of each collision, to the origin of coordinates, the He atom is placed in the xz plane, and that its initial velocity is parallel to the z-axis (collision axis). Then, the PER alignment of J is modeled by initially placing the N_2^+ ion in a randomly oriented plane going through the z-axis (a plane parallel to the collision direction) and the PAR orientation of J is imitated by putting the ion in the xy plane (perpendicular to the collision direction). In both cases, the ion axis is randomly oriented in the respective plane. The NA orientations of the ion are then generated randomly (isotropically) in space.

As is clear from Fig. 7, the values of MTCSs obtained for PAR, PER, and NA J are rather close to one another, which means that the effect of the alignment of J on MTCS is only minor over the whole range of considered collision energies. The only exception is the lowest collision energy, $E_{\mathrm{coll}} = 0.01\,\mathrm{eV}$, for which the difference between both PAR/NA data and PER/NA data is about $\pm 5\,\text{Å}^2$ (but still well below 10 % of the NA value). For CID cross-sections, the differences seem to be much better pronounced if relative deviations are considered, but the absolute magnitudes of the differences are fairly small. Importantly, the CID cross-sections are negligibly small for N_2^+ with both aligned J and non-aligned J.

In general, the PER cross-sections (both MTCSs and CID cross-sections) are below the PAR cross-sections with the NA cross-sections in between. Such an observation is, however, not surprising and quite expected since a) the PER alignment of the N_2^+ angular momentum means that both parallel and perpendicular orientations of the diatomic ion (with respect to the collision axis) are involved while for the PAR alignment, only perpendicularly oriented ions contribute, and b) the effective geometric cross-section of a parallelly oriented diatomic ion is smaller than the geometric cross-section of a perpendicularly oriented one.

It should be also noted that the type 2 MTCSs calculated for PAR and/or PER aligned J (not shown in Fig. 7) are, like for non-aligned J, only marginally different from the corresponding type 1 MTCSs. Observed differences are typically well below 1 % for $E_{\mathrm{coll}} \lesssim 25\,\mathrm{eV}$ and gradually increase up to about 6 % as E_{coll} grows further up. Again, however, very small values of both types of MTCS in this high-energy region are responsible for the increased relative deviations. The magnitudes of the deviations still remain fairly tiny.

4. Conclusions

Collisions of molecular ions of nitrogen, N_2^+, with helium gas have been modeled via the direct dynamics approach [14] based on a classical treatment of atomic nuclei and the use of *ab initio* approaches for potential energy calculations employed on the fly. The main motivation of this work has been to provide quantitative data for macroscopic modeling

of cold helium plasma and its interaction with the environment (air) after the plasma leaves the interior of a plasma generator. The electronic ground state has been presumed in the N_2^+/He collision complex in all points of the collision trajectory and, consequently, the collision dynamics have been treated adiabatically. Electronic excitations have been neglected and the assessment of their role is postponed to a future publication. A broad range of collision energies ($E_{\rm coll} = 0.01 - 100\,{\rm eV}$ in the N_2^+/He center-of-mass system) have been considered to calculate data appropriate for the modeling of interactions between N_2^+ and carrier helium gas in strong electric fields which are present in helium plasma jets [8].

Bunches of trajectories started from properly chosen initial conditions have been integrated numerically and collision cross-sections of the most important processes have been calculated from these trajectories. Forces (gradients of the N_2^+/He ground-state PES) needed to integrate equations of motion have been calculated on the fly using a multi-configuration self-consistent field (MCSCF) method and sufficiently large basis set (aug-cc-pVQZ with atomic orbitals included up to the f-type functions). For selected calculations, analytic representations of the N_2^+/He potential energy surface via artificial neural networks (ANNs) have been used to speed up the calculations. High-quality ANNs have been trained for specific collision energies leading to an almost perfect reproduction of the MCSCF data.

The main outputs of the dynamical calculations are collision cross-sections. Two main collision processes play a role under typical experimental conditions, the non-reactive scattering (NRS) of the N_2^+ ion on helium carrier gas, $N_2^+ + {\rm He} \rightarrow N_2^+ + {\rm He}$, and the collision induced dissociation (CID) of the N_2^+ ion, $N_2^+ + {\rm He} \rightarrow N^+ + N + {\rm He}$. For the NRS process, two kinds of integral cross-sections evaluated at the momentum-transfer (MT) approximation [32] level (Eqs. (4) and (5)) have been considered to remove the well-known issue of the non-integrable singularity of classical differential cross-sections of the elastic scattering channel (included in NRS) at zero deflection angles, while a "usual" integral cross-section has been used for the CID channel (Eq. (6)). The dependence of calculated cross-sections on the initial rotational-vibrational excitation of the N_2^+ ion has been analyzed as well as the effect of the polarization of the N_2^+ angular momentum, a well-known phenomenon in systems with strongly anisotropic interactions [45]. In addition, state-of-the-art experimental data [40, 41, 42] on the mobility of N_2^+ in helium have been inverted via an inverse-method (IM) approach [37] to get "experimental" estimates of the NRS cross-sections for an assessment of the reliability of calculated data and validation of employed computational approaches.

The main results of the present calculation may be summarized as follows. Firstly, a very good correspondence between the theoretical MT cross-sections obtained within the present work and pseudo-experimental MT cross-sections obtained from the IM approach has been achieved at medium-range collision energies ($E_{\rm coll} \approx 0.05 - 2.5\,{\rm eV}$). Only for the lowest collision energy considered here ($E_{\rm coll} = 0.01\,{\rm eV}$) and for energies belonging to the high-energy region ($E_{\rm coll} \gtrsim 2.5\,{\rm eV}$), a well pronounced difference is seen. While for the latter (high collision energies), the IM approach based on a simple isotropic

potential (and, moreover, neglecting the CID channel) may fail to correctly reproduce collision cross-sections, in the former case (low collision energies), the main source of discrepancies may consist in a not fully appropriate inclusion of the induction and dispersion interactions between the N_2^+ ion and He atoms at large distances within the MCSCF method used in the present work. Highly probably, a more accurate treatment of dynamical electron correlations (e.g., a multi-reference CI method) will be needed to remove this discrepancy. **Interestingly, the MTCSs reported in this work for the N_2^+/He collisions agree quite well with recently reported (integral) cross-sections of the N_2^+/e^- scattering [44], even though a different collision system was considered and a different computational methodology was used in Ref. [44].**

Secondly, the effect of the initial rotational-vibrational excitation in N_2^+ on the MT cross-sections is only minor. Even for the highest excitation considered in this paper (j=0,v=10), the deviations are well below 1 Å^2. A bit better pronounced sensitivity is seen for rotational excitations (represented here by j=36,v=0). For example, the MT cross-section deviates, in this case, by about 1.7 Å^2 from the j=0,v=0 value at $E_{\mathrm{coll}} = 0.05\,\mathrm{eV}$, which represents, however, a relative deviation of only 7 %.

Thirdly, the effect of N_2^+ angular momentum alignment on the MT cross-sections is also only moderate and is considerably attenuated as the collision energy increases. As expected from geometric considerations, the parallel alignment of the N_2^+ angular momentum with respect to the direction of collision leads to slightly larger MT cross-sections than the perpendicular alignment, non-polarized data being in between.

Fourthly, the cross-section of the N_2^+ CID is very small over the whole range of collision energies and for all the rotational-vibrational excitations considered. It seems that the CID process is not much important in N_2^+/He collisions, highly probably due to a rather big difference in the masses of nitrogen and helium. In addition, the CID of N_2^+ exhibits rather high energetic threshold ($\gtrsim 10\,\mathrm{eV}$) due to the strong binding in the N_2^+ ion. Naturally, this threshold decreases as the initial rotational-vibrational excitation of the N_2^+ ion increases. At the same time, however, the values of the CID cross-section remain negligibly small ($\sigma_{\mathrm{CID}} \lesssim 0.8\,$Å^2).

Finally, it should be emphasized that though quite a detailed calculation has been performed, many issues concerning N_2^+/He collisions still remain open and require additional investigations. As the most important examples of such issues, let us mention the relaxation of initial rotational-vibrational excitations in the N_2^+ ion or the effect of electronic excitations in the ion on the way the collisions discussed in this work proceed. Both issues will be addressed by our group and will be the subject of prospective studies.

Moreover, one may object that an ultimate test of the accuracy of cross-sections reported in the present work consists in their use in subsequent calculations of the N_2^+/He mobility and a direct comparison of obtained results with available experiments. Such calculations have been performed in our group, together with calculations of other transport properties of the N_2^+ ion in helium which are not available from measurements, and will be the

subject of an immediately following study [31].

Acknowledgments

A support by the Ministry of Education, Youth and Sports of the Czech Republic via the *National Programme of Sustainability II*, project *IT4Innovations excellence in science* (grant no. LQ1602), is greatly acknowledged. The calculations have been performed using the *IT4Innovations* infrastructure supported through the *e-INFRA CZ* project (grant no. ID:90140) and made available to us through computational grants OPEN-16-3, OPEN-16-14, OPEN-17-15, OPEN-17-50, DD-20-23, OPEN-20-34, OPEN-21-46, OPEN-22-21 and OPEN-23-12. One of us (RK) would like to express his thanks to the *PRACE-6IP* project, the EU *Horizon 2020 research and innovation programme* (grant No. 823767), for partial financial support of this work.

References

[1] M. Laroussi. Low-temperature plasmas for medicine? *IEEE Trans. Plasma Sci.*, 37(6):714, June 2009.

[2] M. Yousfi, N. Merbahi, A. Pathak, and O. Eichwald. Low-temperature plasmas at atmospheric pressure: toward new pharmaceutical treatments in medicine. *Fund. Clin. Pharm.*, 28(2):123, February 2014.

[3] H. Tanaka, K. Ishikawa, M. Mizuno, S. Toyokuni, M. Kajiyama, F. Kikkawa and. H.-R. Metelmann, and M. Hori. State of the art in medical applications using non-thermal atmospheric pressure plasma. *Rev. Mod. Plasma Phys.*, 3(1):1, July 2017.

[4] M. Bafoil, A. Jemmat, Y. Martinez ans N. Merbahi, O. Eichwald, C. Dunand, and M. Yousfi. Effects of low temperature plasmas and plasma activated waters on arabidopsis thaliana germination and growth. *PLoS ONE*, 13(4):4, April 2018.

[5] A. Filipić, G. Primc, R. Zaplotnik, N. Mehle, I. Gutierrez-Aguirreand M. Ravnikar, M. Mozetič, J. Žel, and D. Dobnik. Cold atmospheric plasma as a novel method for inactivation of potato virus Y in water samples. *Food Env. Virol.*, 11:220, 2019.

[6] N. Merbahi, G. Ledru, N. Sewraj, and F. Marchal. Electrical behavior and vacuum ultraviolet radiation efficiency of monofilamentary xenon dielectric barrier discharges. *J. Appl. Phys.*, 101(12):123309, June 2007.

[7] P. Muranyi, J. Wunderlich, and M. Heise. Sterilization efficiency of a cascaded dielectric barrier discharge. *J. Appl. Microbiol.*, 103(5):1535, June 2007.

[8] M. Yousfi, A. Hennad, M. Benhenni, O. Eichwald, and N. Merbahi. Basic data of ions in He-air mixtures for fluid modeling of low temperature plasma jets. *J. Appl. Phys.*, 112(4):043301, August 2012.

[9] A. Chicheportiche, B. Lepetit, M. Benhenni, F. X. Gadea, and M. Yousfi. Ab initio transport coefficients of Ar^+ ions in Ar for cold plasma jet modeling. *Phys. Rev. E*, 89(6):063102, jun 2014.

[10] A. Chicheportiche, B. Lepetit, M. Benhenni, F. X. Gadea, and M. Yousfi. Ion collision cross sections and transport coefficients extended to intermediate energies and reduced electric fields for He_2^+ ions colliding with He. *J. Phys. B: At. Mol. Opt. Phys.*, 88(4):043104, oct 2013.

[11] P. M. Mayer and C. Poon. The mechanisms of collisional activation of ions in mass spectrometry. *Canad. Mass Spec.: Gas. Ions*, 28:608–639, 2009.

[12] P. Fournier, C. A. Van de Runstraat, T. R. Govers, J. Schopman, F. J. de Heer, and J. Los.

Collision-induced dissociation of 10 KeV equation N_2^+ ions. Evidence for predissociation of the $C^2\Sigma_u^+$ state. *Chem. Phys. Lett.*, 9:426–428, 1971.

[13] B. E. Fuentes and H. Martinez. Translational spectroscopy of N^+ produced by collision induced dissociation of N_2^+ ion on He and Ar. *Int. J. of Mass Spec.*, 238:55–58, 2004.

[14] W. L. Hase, K. Song, and M. S. Gordon. Direct dynamics simulations. *Comp. Sci. Eng.*, 5(4):36–44, July 2003.

[15] P. O. Dral. Quantum chemistry in the age of machine learning. *J. Phys. Chem. Letters*, 11(6):2336–2347, March 2020.

[16] S. Manzhos and T. Carrington, Jr. Neural network potential energy surfaces for small molecules and reactions. *Chem. Rev.*, 121(16):10187–10217, October 2021.

[17] M. Karplus, R. N. Porter, and R. D. Sharma. Exchange reactions with activation energy. I. Simple barrier potential for (H, H_2). *J. Chem. Phys*, 43(3259):19651, November 1965.

[18] W. H. Press, S. A. Teukolsky, W. T. Vetterling, and B. P. Flannery. *Numerical recipes 3rd edition: The art of scientific computing*. Cambridge University Press, Cambridge, England, August 2007.

[19] R. L. Crane and R. W. Klopfenstein. A predictor-corrector algorithm with an increased range of absolute stability. *J. ACM*, 12(2):227–241, 1965.

[20] F. R. Moulton. *New Methods in Exterior Balistics*. University of Chicago, Chicago, 1926.

[21] J. C. Butcher. A history of Runge-Kutta methods. *Appl Numer Math*, 20(3):247–260, March 1996.

[22] R. J. Le Roy. LEVEL: A computer program for solving the radial Schrödinger equation for bound and quasibound levels. *J Quant Spectrosc Radiat Transf*, 186:167–178, January 2017. Satellite Remote Sensing and Spectroscopy: Joint ACE-Odin Meeting, October 2015.

[23] S. Paláček and R. Kalus. Multidyn 3.0. https://moldyn.vsb.cz/index.php/software-menu?view=article&id=26&catid=2.

[24] H. J. Werner, P. J. Knowles, F. R. Manby, J. A. Black, K. Doll, A. Heßelmann, D. Kats, A. Köhn, T. Korona, D. A. Kreplin, et al. The Molpro quantum chemistry package. *J. Chem. Phys.*, 152(14):144107, 2020.

[25] P. J. Knowles and H.-J. Werner. An efficient second-order MC SCF method for long configuration expansions. *Chem. Phys. Lett.*, 115(3):259–267, 1985.

[26] D. A. Kreplin, P. J. Knowles, and H.-J. Werner. Second-order MCSCF optimization revisited. I. Improved algorithms for fast and robust second-order CASSCF convergence. *J. Chem. Phys*, 150(19):194106, May 2019.

[27] M. Beseda, S. Paláček, R. Kalus, M. Benhenni, M. Yousfi, T. Leininger, and F. X. Gadéa. *Ab initio* approaches for N_2^+ and N_2^+/He ions towards modeling of the N_2^+ ion in cold helium plasma. *Comp. Theor. Chem.*, 1215:113809, 2022.

[28] K. A. Peterson, D. E. Woon, and T. H. Dunning Jr. Benchmark calculations with correlated molecular wave functions. IV. The classical barrier height of the $H + H_2 \rightarrow H_2 + H$ reaction. *J. Chem. Phys*, 100(10):7410–7415, 1994.

[29] K. A. Peterson and T. H. Dunning Jr. Accurate correlation consistent basis sets for molecular core–valence correlation effects: The second row atoms Al–Ar, and the first row atoms B–Ne revisited. *J. Chem. Phys.*, 117(23):10548–10560, 2002.

[30] T. B. Blank and S. D. Brown. Adaptive, global, extended Kalman filters for training feedforward neural networks. *J. Chemom.*, 8(6):391–407, 1994.

[31] S. Paláček, M. Beseda, R. Kalus, M. Benhenni, M. Yousfi, T. Leininger, and F. X. Gadéa. Modeling of the N_2^+ ion in cold helium plasma II: transport properties of N_2^+ in helium. Submitted to Plasma Source Sci. Tech.

[32] M. Child. *Molecular Collision Theory*. Dover Publications, Mineola, N.Y, 1996.

[33] A. Chicheportiche, M. Stachoň, M. Benhenni, F. X. Gadéa, R. Kalus, and M. Yousfi. First principles transport coefficients and reaction rates of Ar_2^+ ions in argon for cold plasma jet modeling. *J. Chem. Phys.*, 141(13):134302, oct 2014.

[34] A. Chicheportiche. *Basic data of atomic and molecular helium and argon ions for the optimization*

of low temperature plasma jets used in the biomedical field. PhD thesis, Université Toulouse III Paul Sabatier, 2014. In French.

[35] C. Van de Steen. *Modeling of transport properties of ions of krypton and xenon for optimization of cold rare-gas plasmas generators.* PhD thesis, Université Toulouse III Paul Sabatier and VSB – Technical University of Ostrava, 2018.

[36] E. A. Mason, H. O'Hara, and F. J. Smith. Mobilities of polyatomic ions in gases: core model. *J. Phys. B: At. Mol. Phys.*, 5(2):169, 1972.

[37] E. A. Mason and E. W. McDaniel. *Transport Properties of Ions in Gases.* John Wiley & Sons, New York, 2005.

[38] L. D. Landau and E. M. Lifshitz. *Quantum mechanics: non-relativistic theory*, volume 3. Elsevier, 2013.

[39] M. Yousfi, A. Hennad, and O. Eichwald. Improved monte carlo method for ion transport in ion-molecule asymmetric systems at high electric fields. *J. Appl. Phys.*, 84(1):107–114, 1998.

[40] M. McFarland, D. L. Albritton, F. C. Fehsenfeld, E. F. Ferguson, and A. L. Schmeltekopf. Flow-drift technique for ion mobility and ion-molecule reaction rate constant measurements. II. positive ion reactions of N^+, O^+, and H_2^+ with O_2 and O^+ with N_2 from thermal to $\approx 2\,\mathrm{eV}$. *J. Chem. Phys.*, 59(12):6620–6628, December 1973.

[41] Y. Kaneko, T. Koizumi, and N. Kobayashi. Mobilities of various ions in non-parent gases; Compilation of the mobility data measured with the injected-ion drift tube mass spectrometer in Tokyo Metropolitan University. *J. Mass. Spec. Soc. Japan*, 26(1):35–52, 1978.

[42] E. B. Anthony, M. J. Bastian, V. M. Bierbaum, and S. R. Leone. Laser probing of rotational-state-dependent velocity distributions of $N_2^+(v'' = 0, j)$ drifted in He. *J. Chem. Phys.*, 112(23):10269, June 2000.

[43] H. W. Ellis, R. Y. Pai, E. W. McDaniel, E. A. Mason, and L. A. Viehland. Transport properties of gaseous ions over a wide energy range. *At. Data Nucl. Data Tables*, 17(3):177, March 1976.

[44] A. Abdoulanziz, C. Argentin, V. Laporta, K. Chakrabarti, A. Bultel, J. Tennyson, I. F. Schneider, and J. Zs. Mezei. Low-energy electron impact dissociative recombination and vibrational transitions of N_2^+. *J. Appl. Phys.*, 129:053303, 2021.

[45] A. J. Orr-Ewing and R. N. Zare. Orientation and alignment of reaction products. *Annu. Rev. Phys. Chem.*, 45(1):315–366, October 1994.

[46] R. A. Dressler, H. Meyer, and S. R. Leone. Laser probing of the rotational alignment of N_2^+ drifted in helium. *J. Chem. Phys.*, 87(10):6029, November 1987.

[47] E. B. Anthony, W. Schade, M. J. Bastian, V. M. Bierbaum, and S. R. Leone. Laser probing of velocity-subgroup dependent rotational alignment of N_2^+ drifted in He. *J. Chem. Phys.*, 106(13):5413, April 1997.

[48] B. Follmeg, P. Rosmus, and H.-J. Werner. Theoretical investigation of collision induced rotational alignment in $N_2^+ - He$. *J. Chem. Phys.*, 93(7):4687, October 1990.

[49] B. Follmeg, H.-J. Werner, and P. Rosmus. On the rotational angular momentum polarization in $N_2^+ - He$. Classical trajectory and hard-ellipsoid model calculations. *J. Chem. Phys.*, 95(2):979, July 1991.

[50] R. Baranowski, B. Wagner, and M. Thachuk. Molecular dynamics study of the collision-induced rotational alignment of N_2^+ drifting in helium. *J. Chem.. Phys.*, 114(15):6662, April 2001.

Figures

Figure 1. Type 1 momentum-transfer cross-sections calculated from selected experimental mobility data via the inverse-method (IM) approach: full line – IM cross-sections obtained from mobility data given in Ref. [40] (as reported in Ref. [43]), dashed line – IM cross-sections based on the mobilities of Ref. [41], and dash-dotted line – IM cross-sections based on Ref. [42]. In the inset, related experimental mobilities are provided for comparison (circles Ref. [40], up triangles Ref. [41], and down triangles Ref. [42]) together with their IM representations (using the same line patterns as in the main panel.)

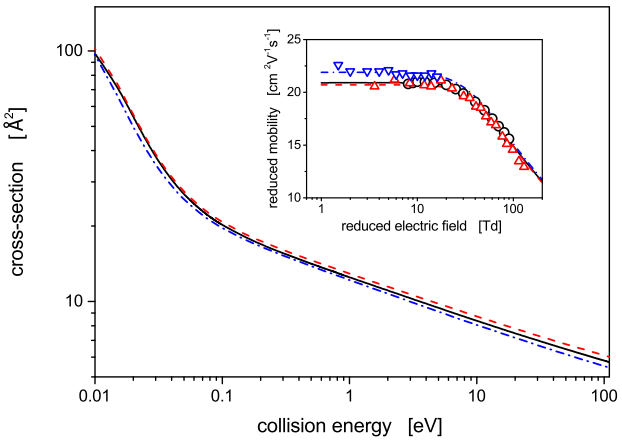

Figure 2. Type 1 momentum-transfer cross-sections (MTCS1) of $N_2^+(j,v) + He \rightarrow N_2^+ + He$ collisions as calculated for selected rotational-vibrational states of the N_2^+ ion at the MCSCF/avqz(spdf) level: full circles j=0,v=0, upper half-filled circles j=0,v=1, lower half-filled circles j=0,v=10, and open circles j=36,v=0. Inverse-method values derived from selected experimental data are also included as gray lines in the background (with the line patterns used as in Fig. 1). **In the inset, deviations of the MTCS1 calculated for the vibrationally and/or rotationally excited N_2^+ ions from the MTCS1 values obtained for j=0,v=0 are depicted.**

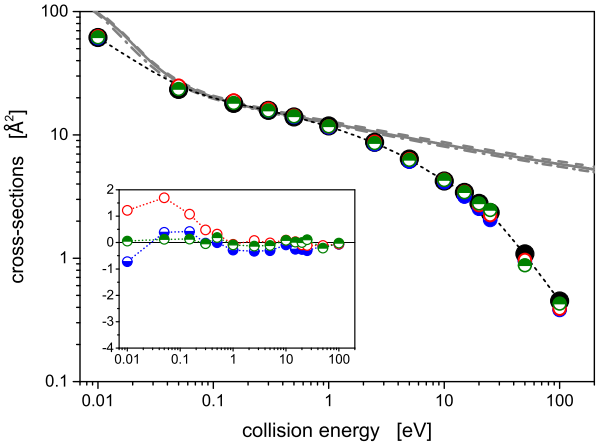

Figure 3. Contributions of particular impact-parameters to type 1 momentum-transfer cross-sections, $2\pi b\Delta\sigma_{\rm NRS}^{\rm (MT1)}(b)$ (see Eq. (7)), of $N_2^+(j=0, v=0)$+He $\rightarrow$ N_2^++He collisions as calculated at the MCSCF/avqz(spdf) level for selected collision energies: full line $E_{\rm coll}$ = 0.01 eV, dashed line $E_{\rm coll}$ = 0.05 eV, and dash-dotted line $E_{\rm coll}$ = 0.15 eV.

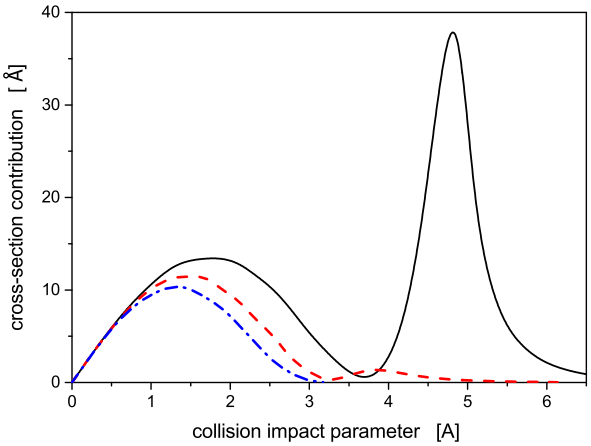

Figure 4. Deviations between type 2 and type 1 momentum-transfer cross-sections **(MTCS2−MTCS1)** of the NRS channel (Eq. (1)) as calculated at the MCSCF/avqz(spdf) level for selected rotational-vibrational states of the N_2^+ ion. The symbols used are the same as in Fig. 2, the connecting lines are added to guide eyes.

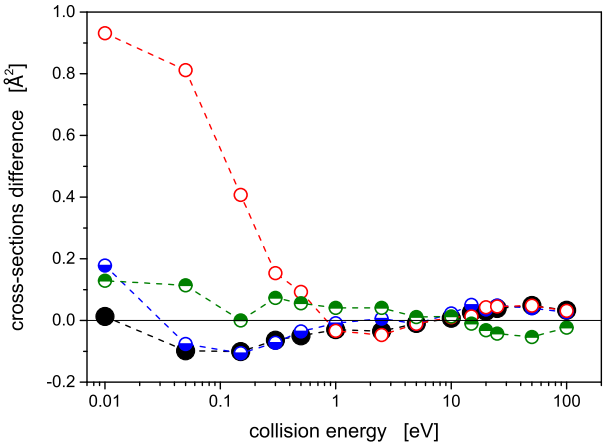

Figure 5. The same as in Fig. 2, but for the collision-induced dissociation cross-sections (Eq. (2)).

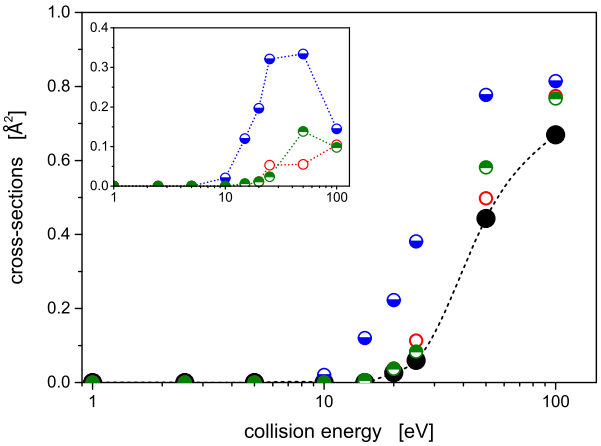

Figure 6. Comparison of type 1 momentum-transfer cross-sections and dissociation cross-sections as obtained for $N_2^+(j{=}0,v{=}0)$/He collisions via the MCSCF/avqz(spdf) method (full and open circles, respectively) and using artificial neural network (ANN) representations of the N_2^+/He potential energy surface (pluses and crosses, respectively). In the inset, deviations between the ANN and MCSCF/avqz(spdf) data **(ANN−MCSCF)** are depicted.

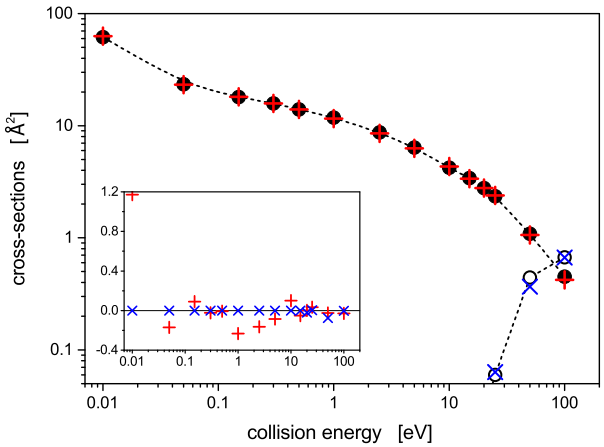

Figure 7. Comparison of type 1 momentum-transfer cross-sections (circles) and collision-induced dissociation cross-sections (diamonds) as obtained for $N_2^+(j{=}0,v{=}0)$/He collisions assuming angular momentum of N_2^+ perpendicularly (PER) and/or parallelly (PAR) aligned to the collision axis (open symbols), and non-aligned (full symbols). For comparison, inverse-method cross-sections are also depicted as grey lines in the background. In the inset, deviations of the PER/PAR cross-sections from the cross-sections calculated for non-aligned N_2^+ are depicted.